

Geophysical Research Letters[®]



RESEARCH LETTER

10.1029/2023GL105201

Key Points:

- Speleothems from southeastern Alaska capture El Niño-Southern Oscillation (ENSO) variability through a teleconnection with the Aleutian Low
- ENSO variability was strongly influenced by solar forcing before ~1970 CE
- ENSO significantly changed properties at ~1970 CE, likely due to anthropogenic forcing

Supporting Information:

Supporting Information may be found in the online version of this article.

Correspondence to:

P. S. Wilcox,
paul.wilcox@uibk.ac.at

Citation:

Wilcox, P. S., Mudelsee, M., Spötl, C., & Edwards, R. L. (2023). Solar forcing of ENSO on century timescales. *Geophysical Research Letters*, 50, e2023GL105201. <https://doi.org/10.1029/2023GL105201>

Received 26 JUN 2023

Accepted 20 SEP 2023

Solar Forcing of ENSO on Century Timescales

Paul S. Wilcox¹ , Manfred Mudelsee² , Christoph Spötl¹ , and R. Lawrence Edwards³

¹Institute of Geology, University of Innsbruck, Innsbruck, Austria, ²Climate Risk Analysis, Bad Gandersheim, Germany,

³Department of Earth Sciences, University of Minnesota, Minneapolis, MN, USA

Abstract Understanding how El Niño-Southern Oscillation (ENSO) responds to natural variability is of key importance for future climate projections under a warming climate. However, there is no clear consensus on what drives ENSO's variability on centennial timescales. Here, we find that the epikarst in southeastern Alaska is effective at filtering ENSO and solar irradiance signals from the Aleutian Low regional climate, which are subsequently recorded in speleothem proxy data. By applying a correlation test, we find that ENSO was significantly influenced by solar irradiance over the past ~3,500 years. This relationship dissolved after ~1970 CE, with ENSO now being dominated by anthropogenic forcing. This implies a new ENSO mean state that will need to be incorporated into future climate projections.

Plain Language Summary Although El Niño-Southern Oscillation (ENSO) is one of the most important climate phenomena globally, it is currently unknown how ENSO responds to natural variability on timescales over 100 years. Natural variability refers to periodic changes in climate due to either solar forcing, the circulation of the atmosphere and ocean, volcanic eruptions, and other factors, irrespective of human intervention. Here, we help solve this problem by studying deposits in caves (speleothems) from Alaska. The speleothems are excellent at capturing atmospheric conditions over the past 3,500 years, and show that solar forcing was significantly controlling ENSO variability. However, the speleothems also show that humans have altered this natural variability, with ENSO entering a new mean state after ~1970 CE.

1. Introduction

El Niño-Southern Oscillation (ENSO) is an important driver of Earth's climate (Deser et al., 2010; McPhaden et al., 2006), fluctuating with significant variability between El Niño (warm phase) and La Niña (cold phase). Instrumental records, only available for the past 150 years, are too short to fully capture ENSO variability on centennial and longer timescales (Stevenson et al., 2012). Paleoclimate proxy techniques attempt to fill this gap by providing ENSO records extending deeper in time. However, these records generally either cover the past few centuries only, lack high temporal resolution, or cover non-continuous intervals of the past millennium.

One of the main uncertainties associated with ENSO variability is the influence of solar forcing. It has been hypothesized that an ocean thermostat response of the tropical Pacific to solar forcing induces both La Niña and El Niño mean states (Clement et al., 1996; Emile-Geay et al., 2007). This hypothesis has found some support in central Pacific corals (Cobb et al., 2003), North American tree rings documenting medieval megadroughts (Cook et al., 2004), and multiproxy climate field reconstructions (Mann et al., 2009). In each of these cases, however, unambiguous confirmation of solar forcing is lacking. This has led some studies to suggest an insignificant response of ENSO to solar forcing, with internal variability being the main driver of ENSO variations (Cobb et al., 2013). Given the rise in anthropogenic warming over the past several decades, it becomes increasingly important to understand the full natural range of ENSO variability and its underlying forcing for improving future climate projections.

The North Pacific provides a unique location to examine ENSO variability through a well-known atmospheric bridge, which links equatorial Pacific and North Pacific climate variability (Alexander et al., 2002; Diaz et al., 2001; Liu & Alexander, 2007) (Figure 1; Figure S1 in Supporting Information S1). The Aleutian Low is the principal climate feature in southeastern Alaska that is influenced by this atmospheric bridge (Alexander et al., 2002; Bjerknes, 1966, 1969), and steers storms and abundant precipitation into the region, especially when strengthened. In general, the link between the equatorial Pacific and the North Pacific is expressed as a stronger-than-normal Aleutian Low during warm sea-surface temperature (SST) anomalies in the equatorial Pacific (i.e., El Niño), and weaker-than-normal Aleutian Low during cool SST anomalies (i.e., La Niña)

© 2023. The Authors.

This is an open access article under the terms of the [Creative Commons Attribution License](https://creativecommons.org/licenses/by/4.0/), which permits use, distribution and reproduction in any medium, provided the original work is properly cited.

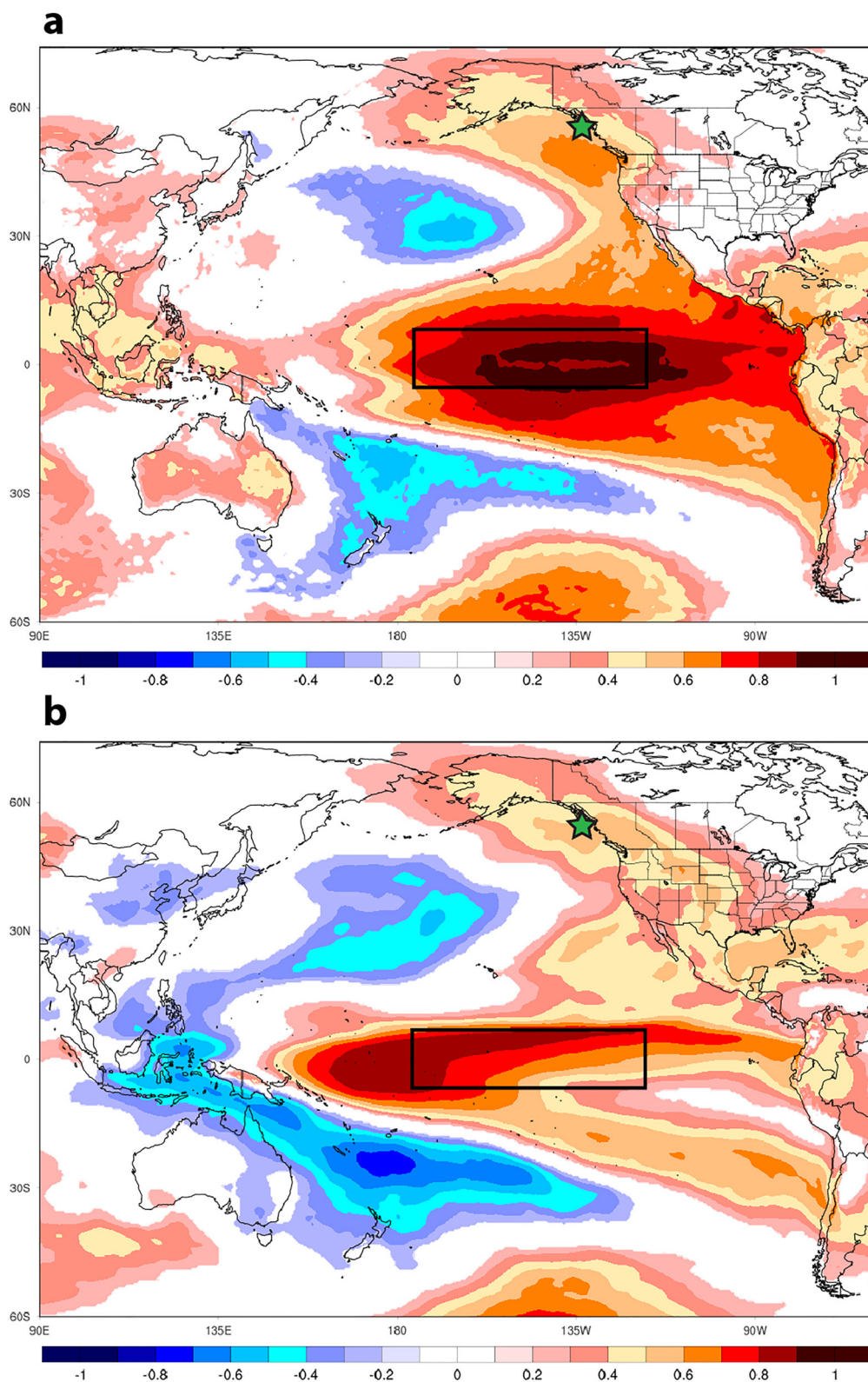


Figure 1. Spatial correlation of ERA5 Reanalysis 2 m temperature (a) and precipitable water (b) with the Niño 3.4 index. Regions of significant correlation are highlighted by color bands (Pearson's correlation [90% CI]). Black box indicates NINO3.4 region, while the speleothem sample location of this study is marked by the green star. Refer to Figure S2 in Supporting Information S1 for a more detailed map of the study area. This plot was generated using Climate Reanalyzer (<http://cci-reanalyzer.org>), Climate Change Institute, University of Maine, USA.

(Alexander et al., 2002; Bjerknes, 1966, 1969). Sea-surface temperatures in the equatorial Pacific, in turn, may be influenced by solar irradiance (Clement et al., 1996; Emile-Geay et al., 2007), which would impact the mean-state of ENSO (Clement et al., 1996; Emile-Geay et al., 2007), and consequently affect the strength of the Aleutian Low via the atmospheric bridge. It has been shown that stronger solar irradiance is generally associated with a weaker Aleutian Low and vice versa (Osterberg et al., 2014). Therefore, there is a known link between both solar irradiance and ENSO and the strength of the Aleutian Low, typically on decadal timescales.

Based on the robust teleconnection between the equatorial Pacific and the North Pacific, we hypothesize that solar irradiance forces ENSO mean state changes which, in turn, force the strength of the Aleutian Low via the atmospheric bridge. In other words, decreased solar irradiance should correspond to an increased frequency of El Niño events and result in an overall strengthened Aleutian Low. Conversely, increased solar irradiance should correspond to an increased frequency of La Niña events and result in an overall weakening of the Aleutian Low. This hypothesis is in agreement with the ocean thermostat mechanism (Clement et al., 1996; Emile-Geay et al., 2007).

Speleothems, which provide long-term, high-resolution reconstructions of climate in the region (Wilcox et al., 2019), offer an untested approach to record the response of changes in the strength of the Aleutian Low, and hence ENSO/solar irradiance, responses in the North Pacific. Here, we utilize speleothems from southeastern Alaska to generate a high-resolution and precisely dated record spanning continuously the past ~3,500 years. Our data demonstrate that the local epikarst in southeastern Alaska is effective at filtering ENSO and solar irradiance signals from the Aleutian Low regional climate. From this, we find that solar forcing has been the primary driver of ENSO variability on centennial timescales, and that this relationship dissolved at ~1970, likely due to anthropogenic forcing.

2. Materials and Methods

2.1. Site Location and Samples

Our data sets were developed from two stalagmites retrieved in spring/summer 2021 in two caves on Prince of Wales Island, located in the temperate rainforest of the southern Alexander Archipelago in Alaska. Klawock, the nearest village to the caves (Figure S2 in Supporting Information S1), has a mean annual air temperature of 7.4°C and receives ~2000 mm of precipitation annually. Speleothem WB-21-5-A is 536 mm in length and was found 50 m inside Wishbone Cave (55.776°N, 133.195°W; 350 m a.s.l.), and WA-21-6-A is 181.5 mm in length and was found 100 m inside Walkabout Cave (55.774°N, -133.191°W; 420 m a.s.l.) (Figure S3 in Supporting Information S1). “Hendy” tests (Hendy, 1971) were performed at four different locations at 2.3, 6.5, 9.9, and 15 cm in WA-21-6-A, and five different locations at 4, 13.8, 25.6, 37.1, and 48 cm in WB-21-5-A to test for isotope equilibrium fractionation (Figure S4 in Supporting Information S1). The fabric texture was identified visually, and shows columnar fabric throughout speleothems, with no evidence of hiatuses.

Interior cave temperatures are a constant 5.6°C for Walkabout Cave, and vary between 2.5 and 8.6°C for Wishbone Cave (Figure S5 in Supporting Information S1). Both speleothems were actively dripping during recovery, suggesting that the speleothem tops are modern. There are no visually detectable hiatuses, and growth rates are constant for both speleothems (Figure S6 in Supporting Information S1). Speleothems WB-21-5-A and WA-21-6-A were sampled for $\delta^{18}\text{O}$ and $\delta^{13}\text{C}$ at 0.5 and 0.25 mm resolution, respectively, producing a temporal resolution of ~2–5 years for both speleothems. Additionally, speleothem WB-21-5-A was sampled for fluid inclusion δD every 0.5 cm, producing a temperature record with a resolution of ~40 years (Figure S7 in Supporting Information S1).

2.2. U-Th Ages

A total of 10 powdered calcite samples were manually drilled for U-Th dating under a laminar flow hood; 5 from WA-21-6-A, and 5 from WB-21-5-A (Figure S3 in Supporting Information S1) (Wilcox et al., 2022). U-Th samples were processed at the University of Minnesota Trace Metal Isotope Geochemistry Lab and analyzed using a ThermoFisher Neptune Plus multi-collector inductively coupled plasma mass spectrometer equipped with an Aridus desolvation nebulizer, following the method of Shen et al. (2012). Ages are reported with 2σ errors in BCE/CE. A time-depth model was created in OxCal 4.4 using the Bayesian approach (Bronk Ramsey, 2008, 2009; Bronk Ramsey & Lee, 2013).

2.3. Stable Isotopes

A total of 1800 stable isotope locations were drilled using a Merchantek micromill. In WA-21-6-A, samples were drilled every 0.25 mm, yielding a temporal resolution of ~ 5 years. Samples in WB-21-5-A were drilled every 0.5 mm, yielding a temporal resolution of ~ 2 –5 years. Stable isotope samples were analyzed at the University of Innsbruck using a ThermoFisher Delta V isotope ratio mass spectrometer equipped with a Gasbench II (Spötl, 2011). Stable isotopes are reported in per mil relative to Vienna Pee Dee Belemnite (VPDB). Long-term analytical precision is less than or equal to 0.08‰ for both $\delta^{13}\text{C}$ and $\delta^{18}\text{O}$ (1σ).

2.4. Fluid Inclusions

Speleothem fluid inclusion water isotopes were analyzed at the University of Innsbruck using a continuous-flow technique via high-temperature reduction on glassy carbon (Dublyansky & Spötl, 2009). $\delta\text{D}_{\text{fi}}$ isotope ratios are given in per mil (‰) using the standard delta notation and are reported relative to the Vienna Standard Mean Ocean Water. We extracted 95 calcite blocks from 87 different depths, weighing between 1 and 1.5 g, from the central growth axis of stalagmite WB-21-5-A. Replicates were produced at 0.5, 10.5, 20.5, 30.5, and 40.5 cm depth. See (Dublyansky & Spötl, 2009) for details on the crushing procedure. The precision of replicate measurements of our in-house calcite standard is typically 1.5‰ for $\delta\text{D}_{\text{fi}}$ for water amounts between 0.1 and 1 μl . Because crushing of our calcite samples released up to 1 μl of water (mean 0.40 μl), the precision of 1.5‰ for $\delta\text{D}_{\text{fi}}$ was found to be adequate for this study. Temporal resolution is ~ 40 years.

The paleotemperature record of stalagmite WB-21-5-A was reconstructed based on the modern-day regional water isotope-temperature relationship (Rozanski et al., 1992). Only $\delta\text{D}_{\text{fi}}$ values were used for calculating paleotemperatures for the following reasons: post-depositional processes can alter the original $\delta^{18}\text{O}_{\text{fi}}$ in fluid inclusion water and thus limit the use of $\delta^{18}\text{O}_{\text{fi}}$ for paleotemperature calculations (McDermott, 2004). In addition, $\delta\text{D}_{\text{fi}}$ is not affected by isotopic fractionation during calcite precipitation and remains unaltered as there is no hydrogen source once the water is entrapped in the calcite matrix. We used the global meteoric water line ($\delta\text{D} = 8 \cdot \delta^{18}\text{O} + 10\text{‰}$) to convert $\delta\text{D}_{\text{fi}}$ to $\delta^{18}\text{O}_{\text{calculated}}$. Modern-day drip-water yielded a $\delta^{18}\text{O}$ value of -10‰ which was used as the modern-day $\delta^{18}\text{O}$ anchor point. Fluid inclusion $\delta^{18}\text{O}_{\text{calculated}}$ values were subtracted from this modern-day $\delta^{18}\text{O}$ anchor point to obtain $\delta^{18}\text{O}_{\text{difference}}$. Next, a temperature- $\delta^{18}\text{O}$ transfer function (TF) was used to convert $\delta^{18}\text{O}_{\text{difference}}$ into temperature. Because it is unclear which TF is appropriate, we evaluated a range of possible values, between 0.26 and 0.36 ‰/°C, which represents the error range of the south-central Alaska temperature- $\delta^{18}\text{O}$ slope of 0.31 ‰/°C (Bailey et al., 2019). Because there is a minor 0.1°C difference in temperatures calculated from the range of TF values, we report temperatures based on the TF of 0.31 ‰/°C. Finally, we subtracted the mean annual temperature of a nearby weather station in Klawock (55.555°N, 133.096°W; 24 m a.s.l.—Figure S2 in Supporting Information S1) of 7.4°C (Western Regional Climate Center) to obtain paleotemperature anomaly values:

$$T = 7.4 - [-10 - \delta^{18}\text{O}_{\text{calculated}}] * \text{TF} \quad (1)$$

A regional lapse rate likely causes cooler mean annual temperatures at the cave sites ~ 400 m higher in elevation, probably closer to the interior cave temperatures of Walkabout Cave ($\sim 5.6^\circ\text{C}$) (Figure S5 in Supporting Information S1). In lieu of using unavailable long-term site-specific temperature data, we report temperature data as anomalies versus weather station Klawock (Figure 3; Figure S7 in Supporting Information S1).

Uncertainties reflect isotope measurement errors, and one standard deviation of repeated measurements. The uncertainties are applied through all steps of the paleotemperature calculation. Further, uncertainties are propagated between sampling locations.

2.5. Cave Monitoring

HOB0 Pro v2 temperature loggers (accuracy: $\pm 0.21^\circ\text{C}$) were placed near the entrance of both Walkabout and Wishbone Caves, and near the extracted stalagmites. Temperature was measured at 1-hr intervals for 1 year, starting when the stalagmites were extracted (Figure S5 in Supporting Information S1).

A Stalagmite drip logger was placed directly where stalagmite WA-21-6-A was extracted, and recorded drip counts at 1-hr intervals for 1 year, starting when the stalagmite was extracted (Figure S5 in Supporting Information S1).

2.6. Statistical Analyses

For correlation estimation on two time series that are not observed on the same timescale, the “binned correlation coefficient” was used (Mudelsee, 2014). This measure equals Pearson's correlation coefficient calculated on the respective averages within time bins of the two-time series. The optimal binwidth was obtained using the software TAUEST (Mudelsee, 2002), the temporal spacings of the two series, and the binwidth formula after (Mudelsee, 2014). The uncertainty of the estimated binned correlation coefficients was determined by calibration of 90% Student's *t* confidence intervals using the software PearsonT3 (Ólafsdóttir & Mudelsee, 2014). It should be noted that a confidence interval (for an estimation) is an uncertainty measure that is superior to a *p*-value (for a hypothesis test) because it carries more quantitative information. That means a confidence interval is for a statement about the strength of an association, not merely whether there is one (Efron & Tibshirani, 1993; Yates, 1951). Furthermore, the suitability of this correlation method to climate data and its validity have been demonstrated by means of observed and artificial series (Mudelsee, 2014).

The spectra for the records were estimated on the detrended time series obtained with a Gasser–Müller nonparametric trend (Mudelsee, 2014) calculated with a bandwidth of 500 years in order to exclude distortions from long-term variations. The spectral power was determined by means of the Lomb–Scargle Fourier transform combined with Welch's overlapped segment averaging procedure (Mudelsee, 2014), which is implemented in REDFIT software (Schulz & Mudelsee, 2002). To determine a frequency-dependent correct factor for estimation bias stemming from the uneven spacings, we conducted 10,000 Monte Carlo simulations of an AR(1) red-noise process. The time interval (in years BCE/CE) equals [−2386.5; 2021.5] (WA-21-6-A $\delta^{18}\text{O}$) or [−1600.2; 2021.5] (WB-21-5-A $\delta^{18}\text{O}$) and the number of data points, from which the average time resolution can be calculated, equals 727 (WA-21-6-A $\delta^{18}\text{O}$) or 1073 (WB-21-5-A $\delta^{18}\text{O}$). Further spectrum estimation parameters (Schulz & Mudelsee, 2002) were: oversampling factor 64, highest-frequency factor 1.0, Welch I data taper, predefined equivalent autocorrelation coefficient (Schulz & Mudelsee, 2002) equal to 0.6632 (WA-21-6-A $\delta^{18}\text{O}$; Figure S8 in Supporting Information S1) or 0.7909 (WB-21-5-A $\delta^{18}\text{O}$; Figure S8 in Supporting Information S1), and number of segments equal to 17 (WA-21-6-A $\delta^{18}\text{O}$) or 13 (WB-21-5-A $\delta^{18}\text{O}$) in order to yield comparable 6-dB spectral resolution bandwidths for the two records. The significances of the spectral peaks were tested against the upper 99% level from the chi-squared distribution for the AR(1) alternative.

3. Results

3.1. Controls on Speleothem $\delta^{18}\text{O}$

A pseudo amount effect in combination with changing source regions are likely the dominant controls on $\delta^{18}\text{O}$ in precipitation at the cave sites, as indicated by a regional comparison of modern precipitation (Figure S9 in Supporting Information S1). Essentially, a strengthened Aleutian Low will draw more moisture meridionally from southern regions (Liu & Alexander, 2007), which has relatively low $\delta^{18}\text{O}$ values (Bailey et al., 2019). A strengthened Aleutian Low will also contribute to higher rainfall amounts at the cave sites, resulting in more depleted $\delta^{18}\text{O}$ values, and hence, a pseudo amount effect. On the other hand, a weakened Aleutian Low will draw an increased fraction of moisture from zonal regions, which has relatively high $\delta^{18}\text{O}$ values (Bailey et al., 2019). A weaker Aleutian Low will also cause lower rainfall amounts at the cave sites, resulting in more enriched $\delta^{18}\text{O}$ values. We can reasonably exclude topographic barriers as dominant controls on $\delta^{18}\text{O}$ in precipitation as there are no topographic barriers between the cave sites and the Pacific Ocean to cause isotopic depletion. Further, there is a weak relationship between changes in air temperature and $\delta^{18}\text{O}$ of precipitation in southcentral Alaska, with surface air temperatures explaining only ~30% of variability in the $\delta^{18}\text{O}$ precipitation data (Bailey et al., 2019). Although there are no networks monitoring isotopes in southeastern Alaska, the region as a whole is strongly influenced by the Aleutian Low (Bailey et al., 2019) and likely has a similar weak relationship between air temperature and $\delta^{18}\text{O}$ of precipitation. Therefore, we argue that $\delta^{18}\text{O}$ of calcite is dominantly controlled by the amount of precipitation in combination with the source region, with depleted isotope values indicating more precipitation and a southerly derived source region, and vice versa. This is corroborated by drip rate data from the site of speleothem WA-21-6-A, which closely mirrors local precipitation amounts (Figure S5 in Supporting Information S1).

A pseudo amount effect and changing source regions controlling $\delta^{18}\text{O}$ in precipitation at the cave sites implies that speleothem oxygen isotopes are a reliable proxy to determine the strength of the Aleutian Low. Depleted speleothem $\delta^{18}\text{O}$ indicates a strengthened Aleutian Low, and vice versa, consistent with regional lake proxy data (Anderson et al., 2005) and ice core data (Osterberg et al., 2014). To test if ENSO and solar irradiance signals

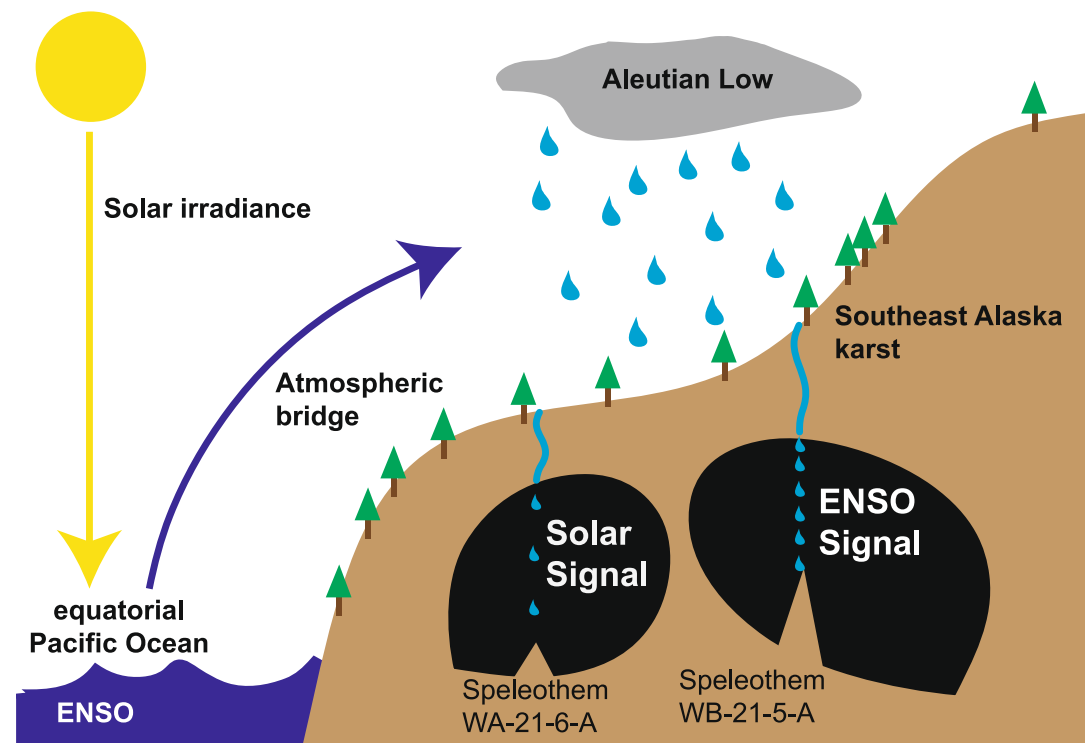


Figure 2. Schematic illustrating how the Aleutian Low is forced by both solar irradiance and El Niño-Southern Oscillation (ENSO) through the atmospheric bridge. The epikarst is effective at filtering the regional Aleutian Low climate into either the solar irradiance or ENSO signals.

can be extracted from speleothem $\delta^{18}\text{O}$, we applied the binned correlation coefficient (r) to find reliable statistical linkages among pairs of proxy data on unequal timescales (Mudelsee, 2014) (see methods for details on the statistics). First, we examine correlations between speleothem data, and then apply the correlation test with solar irradiance and ENSO proxy data.

3.2. Speleothem Proxy Correlations

For speleothem WB-21-5-A, we find that the fluid inclusion temperature reconstruction correlates significantly with $\delta^{18}\text{O}$ at $r = 0.59$ with a 90% calibrated bootstrap confidence interval of [0.43; 0.71] (Figure S10 in Supporting Information S1). The $\delta^{18}\text{O}$ series from speleothems WA-21-6-A and WB-21-5-A are significantly correlative, $r = 0.25$ [0.01; 0.45] (Figure S10 in Supporting Information S1), highlighting regional consistencies that would be expected between neighboring speleothem $\delta^{18}\text{O}$ data that precipitated close to isotopic equilibrium with the drip water (Figure S4 in Supporting Information S1). We argue that deviations between speleothem $\delta^{18}\text{O}$ are a result of spectral frequency differences between sites (Figure S8 in Supporting Information S1), with speleothem WB-21-5-A recording a high-frequency $\delta^{18}\text{O}$ signal and WA-21-6-A recording a low-frequency $\delta^{18}\text{O}$ signal (Figure S11 in Supporting Information S1). This is likely the result of the large difference in growth rate (Figure S6 in Supporting Information S1), and hence drip rate, between the two sites. Since drip water transports the $\delta^{18}\text{O}$ signal from the soil zone to the speleothem site, different drip rates will lead to different $\delta^{18}\text{O}$ frequencies at each speleothem site. We hypothesize that the local epikarst acts as a low-pass filter, resulting in a modulation of the Aleutian Low regional climate signal (Figure 2). In speleothem WA-21-6-A, we observe a climate signal that is potentially linked with total solar irradiance (TSI), while in speleothem WB-21-5-A, we observe a climate signal that is potentially linked with ENSO. We then explore the statistical significance of these potential climate linkages to determine if they are robust.

3.3. Solar Irradiance and ENSO Correlations

To determine if the $\delta^{18}\text{O}$ series from speleothem WA-21-6-A is statistically linked with TSI, we compared the $\delta^{18}\text{O}$ proxy to the most up-to-date physics-based reconstruction of TSI currently available (Wu et al., 2018) (Figure 3). We find that TSI correlates significantly with speleothem WA-21-6-A $\delta^{18}\text{O}$ after ~ 0 CE at $r = 0.52$

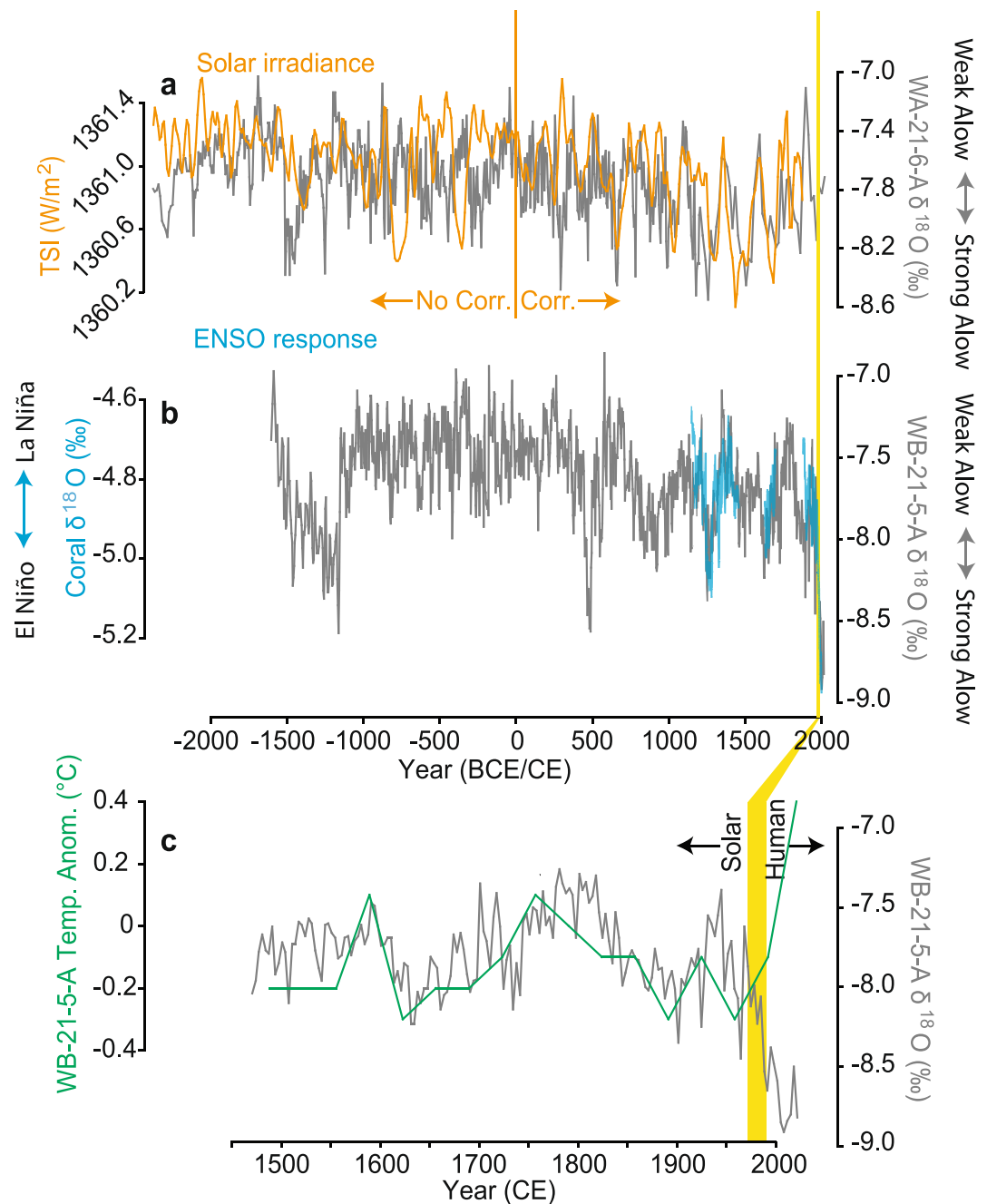


Figure 3. Southeastern Alaska speleothem record compared with solar irradiance and El Niño-Southern Oscillation (ENSO) proxy data. (a) Speleothem WA-21-6-A $\delta^{18}\text{O}$ versus total solar irradiance (TSI) (Wu et al., 2018). Orange line denotes timing of correlation differences between TSI and WA-21-6-A, with significant correlation after 0 CE and no significant correlation before 0 CE; (b) Speleothem WB-21-5-A $\delta^{18}\text{O}$ versus coral $\delta^{18}\text{O}$ (Dee et al., 2020). Allow = Aleutian Low; (c) Magnified time interval comparing speleothem WB-21-5-A $\delta^{18}\text{O}$ and temperature anomalies. Refer to Figure S6 in Supporting Information S1 for an extended temperature plot. In (a–c) yellow bar highlights North Pacific regime shift, when ENSO is disconnected from solar forcing and anthropogenic forcing takes over.

[0.32; 0.68] (Figure S10 in Supporting Information S1), with decreased solar irradiance correlating with a strengthened Aleutian Low in speleothem WA-21-6-A, and vice versa. However, we find no significant correlation prior to ~0 CE. The lack of correlation for the earlier part could be due to proxy bias, with all previous TSI reconstructions dependent on ^{14}C and ^{10}Be data. Additionally, we performed a spectral analysis, which shows solar cycles (Moussas et al., 2005) at all 3 spectral peaks of 16-, 19-, and 28-year periods (Figure S8 in Supporting

Information S1), providing enhanced confidence that speleothem WA-21-6-A reliably records TSI variability. However, due to the lack of correlation prior to ~0 CE, we only provide interpretations for the past ~2000 years.

To determine if the $\delta^{18}\text{O}$ series from speleothem WB-21-5-A is statistically linked with ENSO, we compared the $\delta^{18}\text{O}$ proxy to an ENSO reconstruction produced from a coral $\delta^{18}\text{O}$ record in the central tropical Pacific spanning the past ~750 years (23) (Figure 3). We find that the coral $\delta^{18}\text{O}$ (Dee et al., 2020) is significantly correlated with speleothem WB-21-5-A at $r = 0.54$ [0.10; 0.80] (Figure S10 in Supporting Information S1), with increased frequency of El Niño events correlating with a strengthened Aleutian Low in speleothem WB-21-5-A, and vice versa for La Niña events (Figure 3). Additionally, we performed a spectral analysis, which shows the “classical” ENSO power (Allen, 2000) at the 7.2-year period (Figure S8 in Supporting Information S1), which is added confidence that speleothem WB-21-5-A reliably records ENSO variability.

The correlation tests confirm that the strength of the Aleutian Low correlates significantly with either solar irradiance or ENSO. And, since speleothem WA-21-6-A $\delta^{18}\text{O}$ (solar irradiance signal) and WB-21-5-A $\delta^{18}\text{O}$ (ENSO signal) are significantly correlated, this provides compelling evidence that solar irradiance can influence ENSO mean state changes. More specifically, it agrees with our hypothesis that solar irradiance forces ENSO mean state changes which, in turn, force the strength of the Aleutian Low via the atmospheric bridge (Figure 2). Our data thus supports the ocean thermostat mechanism (Clement et al., 1996; Emile-Geay et al., 2007) before 1970 CE. After 1970 CE, ENSO deviates from natural variability based on the divergent trends of temperature and precipitation (Figure 3).

4. Discussion

Our data shows that solar forcing can have an influence on ENSO mean state changes on centennial timescales over the past 2,000 years. Notably, this confirms the ocean thermostat mechanism whereby solar irradiance induces changes in the east-west temperature gradient of the tropical Pacific and, hence, ENSO activity (Clement et al., 1996; Emile-Geay et al., 2007). In general, periods of increased solar irradiance correspond to an increased frequency of La Niña events, while decreased solar irradiance corresponds to an increased frequency of El Niño events (Figure 3). Only the El Niño mean state change at ~500 CE does not fully agree with solar irradiance (Figure 3), and may be associated with the strongest volcanic eruption in the past 2,500 years (Sigl et al., 2015). This event is in conjunction with one of the most extensive regional glacial advances in the past 2000 years (Sigl et al., 2015), and may correspond to the Late Antique Little Ice Age, whereby unprecedented summer cooling is recorded by tree rings in Europe (Büntgen et al., 2016). Therefore, we find that ENSO mean state changes are mostly insensitive to volcanic eruptions, consistent with coral reconstructions (Dee et al., 2020), except for exceedingly rare super-eruptions such as the ~500 CE eruption.

In southeastern Alaska on centennial timescales, warm/dry conditions correspond to La Niña mean states and cool/wet conditions correspond to El Niño mean states. While we recognize that modern instrumental data in the region (Figure S1 in Supporting Information S1) indicates warm/wet conditions during individual El Niño events and cool/dry conditions for individual La Niña events on interannual timescales, we suggest that this does not take into account long term trends. For example, the expected increase in cloudy conditions, which have a net cooling effect (Peirrehumbert, 2010), during an El Niño mean state would probably lower the regional temperature on centennial timescales, and vice versa for La Niña events. This is corroborated by regional glacial retreats/advances in the region, which follow the long term trend of El Niño during glacial advances and the long term trend of La Niña during glacial retreats (Figure S12 in Supporting Information S1) (Wiles et al., 2008).

Atmospheric CO_2 strongly disconnects from the natural variability of the speleothem record after ~1850 CE (Figure S13 in Supporting Information S1), in agreement with the rise of CO_2 above pre-industrial levels (Ahn et al., 2012). This is notable, given that the equatorial Pacific represents the largest CO_2 source globally (Takahashi et al., 2009), and is clearly at odds with natural forcings indicated by the speleothem record. Given the insignificant increase in solar irradiance to such a remarkable rise in atmospheric CO_2 , it is obvious that anthropogenic greenhouse gases are responsible for the deviation from natural variability. We suggest that this resulted in the breakdown of the ocean thermostat mechanism in the 1970s, in conjunction with a well-documented ENSO and North Pacific regime shifts in the late 1970s (Diaz et al., 2001; Giamalaki et al., 2018; Graham, 1994; Hare & Mantua, 2000; Mayo & March 1990). This has resulted in increasingly warmer/wetter conditions in south-east Alaska unseen during the previous ~3,500 years. The warm/wet combination is inconsistent with previous

regional El Niño or La Niña mean-state responses, and indicates a significant change in ENSO properties (Freund et al., 2019; Graham, 1994; Wang et al., 2019).

While the regime shifts in the late 1970s could also be attributed to a disruption in the atmospheric bridge linking the equatorial Pacific to the North Pacific, we argue that this is unlikely given the significant correlation between modern-day instrumental records of ENSO and regional southeastern Alaska precipitation/temperature (Figure S1 in Supporting Information S1). This implies that the atmospheric bridge is still strong, with ENSO continuing to force the strength of the Aleutian Low even under increased greenhouse gases.

We suggest that a switch to the weaker Walker mechanism in the 1970s, whereby zonal tropical sea-surface temperatures are reduced (Vecchi et al., 2008), resulted in the mean state shift of ENSO. Based on our speleothem data, the switch to a weaker Walker mechanism in the 1970s would not be possible if driven by natural forcings alone, and required the input of anthropogenic greenhouse gases. Reduced zonal tropical sea-surface temperatures have led to an El Niño mean-state and a strengthened Aleutian Low, bringing increased precipitation. However, the regional atmospheric warming in conjunction with the increased precipitation is atypical of an El Niño mean-state on centennial timescales. This implies that the wet/cool conditions typical of El Niño mean-state and associated with glacial advances during past centuries is being overwhelmed by anthropogenic warming. This significant change in ENSO may suggest that a climate change tipping point may have been crossed in the 1970s. We recommend that climate models fix biases that will result in both a diminished ocean thermostat response and an increased weaker Walker response at ~1970 CE for improved climate projections of ENSO.

Data Availability Statement

U-Th, fluid inclusion, and stable isotope data in the study are available at Wilcox et al. (2022) (<https://doi.org/10.1594/PANGAEA.949778>).

Acknowledgments

This work was funded by the Austrian Science Fund (FWF) Grant P338960 to P.S.W. We are grateful for the Anna Harris, Jim Baichtal, Christian DeCelle, and the Tongass National Forest Geology program for their continued support for this work. Additionally, extensive stable isotope sampling used in this manuscript was conducted by Jessica Honkonen. Finally, we would like to thank the reviewers for their insightful feedback.

References

- Ahn, J., Brook, E. J., Mitchell, L., Rosen, J., McConnell, J. R., Taylor, K., et al. (2012). Atmospheric CO₂ over the last 1000 years: A high-resolution record from the West Antarctic Ice Sheet (WAIS) divide ice core. *Global Biogeochemical Cycles*, 26(2), GB2027. <https://doi.org/10.1029/2011gb004247>
- Alexander, M. A., Bladé, I., Newman, M., Lanzante, J. R., Lau, N. C., & Scott, J. D. (2002). The atmospheric bridge: The influence of ENSO teleconnections on air–sea interaction over the global oceans. *Journal of Climate*, 15(16), 2205–2231. [https://doi.org/10.1175/1520-0442\(2002\)015<2205:tabtio>2.0.co;2](https://doi.org/10.1175/1520-0442(2002)015<2205:tabtio>2.0.co;2)
- Allan, R. J. (2000). ENSO and climatic variability in the past 150 years. In H. F. Diaz & V. Markgraf (Eds.), *ENSO: Multiscale variability and global and regional impacts* (pp. 3–55). Cambridge University Press.
- Anderson, L., Abbott, M. B., Finney, B. P., & Burns, S. J. (2005). Regional atmospheric circulation change in the North Pacific during the Holocene inferred from lacustrine carbonate oxygen isotopes, Yukon Territory, Canada. *Quaternary Research*, 64, 21–35. <https://doi.org/10.1016/j.yqres.2005.03.008>
- Bailey, H. L., Klein, E. S., & Welker, J. M. (2019). Synoptic and mesoscale mechanisms drive winter precipitation δ¹⁸O/δ²H in south-central Alaska. *Journal of Geophysical Research-Atmospheres*, 124(7), 4252–4266. <https://doi.org/10.1029/2018jd030050>
- Bjerknes, J. (1966). A possible response of the atmospheric Hadley circulation to equatorial anomalies of ocean temperature. *Tellus*, 18(4), 820–829. <https://doi.org/10.1111/j.2153-3490.1966.tb00303.x>
- Bjerknes, J. (1969). Atmospheric teleconnections from the equatorial Pacific. *Monthly Weather Review*, 97(3), 163–172. [https://doi.org/10.1175/1520-0493\(1969\)097<0163:atftpe>2.3.co;2](https://doi.org/10.1175/1520-0493(1969)097<0163:atftpe>2.3.co;2)
- Bronk Ramsey, C. (2008). Deposition models for chronological records. *Quaternary Science Reviews*, 27(1–2), 42–60. <https://doi.org/10.1016/j.quascirev.2007.01.019>
- Bronk Ramsey, C. (2009). Bayesian analysis of radiocarbon dates. *Radiocarbon*, 51(1), 337–360. <https://doi.org/10.1017/s0033822200033865>
- Bronk Ramsey, C., & Lee, S. (2013). Recent and planned developments of the program OxCal. *Radiocarbon*, 55(2), 720–730. <https://doi.org/10.1017/s0033822200057878>
- Büntgen, U., Myglan, V. S., Ljungqvist, F. C., McCormick, M., Di Cosmo, N., Sigl, M., et al. (2016). Cooling and societal change during the late antique little ice age from 536 to around 660 AD. *Nature Geoscience*, 9(3), 231–236. <https://doi.org/10.1038/ngeo2652>
- Clement, A. C., Seager, R., Cane, M. A., & Zebiak, S. E. (1996). An ocean dynamical thermostat. *Journal of Climate*, 9, 2190–2196. [https://doi.org/10.1175/1520-0442\(1996\)009<2190:aodt>2.0.co;2](https://doi.org/10.1175/1520-0442(1996)009<2190:aodt>2.0.co;2)
- Cobb, K. M., Charles, C. D., Cheng, H., & Edwards, R. L. (2003). El Niño/Southern Oscillation and tropical Pacific climate during the last millennium. *Nature*, 424(6946), 271–276. <https://doi.org/10.1038/nature01779>
- Cobb, K. M., Westphal, N., Sayani, H. R., Watson, J. T., Di Lorenzo, E., Cheng, H., et al. (2013). Highly variable El Niño–southern oscillation throughout the Holocene. *Science*, 339(6115), 67–70. <https://doi.org/10.1126/science.1228246>
- Cook, E. R., Woodhouse, C. A., Eakin, C. M., Meko, D. M., & Stahle, D. W. (2004). Long-term aridity changes in the western United States. *Science*, 306(5698), 1015–1018. <https://doi.org/10.1126/science.1102586>
- Dee, S. G., Cobb, K. M., Emile-Geay, J., Ault, T. R., Edwards, R. L., Cheng, H., & Charles, C. D. (2020). No consistent ENSO response to volcanic forcing over the last millennium. *Science*, 367(6485), 1477–1481. <https://doi.org/10.1126/science.aax2000>
- Deser, C., Alexander, M. A., Xie, S. P., & Phillips, A. S. (2010). Sea surface temperature variability: Patterns and mechanisms. *Annual Review of Marine Science*, 2(1), 115–143. <https://doi.org/10.1146/annurev-marine-120408-151453>

- Diaz, H. F., Hoerling, M. P., & Eischeid, J. K. (2001). ENSO variability, teleconnections and climate change. *International Journal of Climatology*, 21(15), 1845–1862. <https://doi.org/10.1002/joc.631>
- Dublyansky, Y. V., & Spötl, C. (2009). Hydrogen and oxygen isotopes of water from inclusions in minerals: Design of a new crushing system and on-line continuous-flow isotope ratio mass spectrometric analysis. *Rapid Communications in Mass Spectrometry*, 23(17), 2605–2613. <https://doi.org/10.1002/rcm.4155>
- Efron, B., & Tibshirani, R. J. (1993). *An introduction to the bootstrap*. Chapman and Hall.
- Emile-Geay, J., Cane, M., Seager, R., Kaplan, A., & Almasi, P. (2007). El Niño as a mediator of the solar influence on climate. *Paleoceanography*, 22(3), PA3210. <https://doi.org/10.1029/2006pa001304>
- Freund, M. B., Henley, B. J., Karoly, D. J., McGregor, H. V., Abram, N. J., & Dommeneget, D. (2019). Higher frequency of Central Pacific El Niño events in recent decades relative to past centuries. *Nature Geoscience*, 12(6), 450–455. <https://doi.org/10.1038/s41561-019-0353-3>
- Giamalaki, K., Beaulieu, C., Faranda, D., Henson, S. A., Josey, S. A., & Martin, A. P. (2018). Signatures of the 1976–1977 regime shift in the North Pacific revealed by statistical analysis. *Journal of Geophysical Research-Oceans*, 123(6), 4388–4397. <https://doi.org/10.1029/2017jc013718>
- Graham, N. E. (1994). Decadal-scale climate variability in the tropical and North Pacific during the 1970s and 1980s: Observations and model results. *Climate Dynamics*, 10(3), 135–162. <https://doi.org/10.1007/bf00210626>
- Hare, S. R., & Mantua, N. J. (2000). Empirical evidence for North Pacific regime shifts in 1977 and 1989. *Progress in Oceanography*, 47(2–4), 103–145. [https://doi.org/10.1016/s0079-6611\(00\)00033-1](https://doi.org/10.1016/s0079-6611(00)00033-1)
- Hendy, C. H. (1971). The isotopic geochemistry of speleothems—I. The calculation of the effects of different modes of formation on the isotopic composition of speleothems and their applicability as palaeoclimatic indicators. *Geochimica et Cosmochimica Acta*, 35(8), 801–824. [https://doi.org/10.1016/0016-7037\(71\)90127-x](https://doi.org/10.1016/0016-7037(71)90127-x)
- Liu, Z., & Alexander, M. (2007). Atmospheric bridge, oceanic tunnel, and global climatic teleconnections. *Reviews of Geophysics*, 45(2), RG2005. <https://doi.org/10.1029/2005rg000172>
- Mann, M. E., Zhang, Z., Rutherford, S., Bradley, R. S., Hughes, M. K., Shindell, D., et al. (2009). Global signatures and dynamical origins of the little ice age and medieval climate anomaly. *Science*, 326(5957), 1256–1260. <https://doi.org/10.1126/science.1177303>
- Mayo, L. R., & March, R. S. (1990). Air temperature and precipitation at Wolverine Glacier, Alaska; Glacier growth in a warmer, wetter climate. *Annals of Glaciology*, 14, 191–194. <https://doi.org/10.1017/s0260305500008557>
- McDermott, F. (2004). Palaeo-climate reconstruction from stable isotope variations in speleothems: A review. *Quaternary Science Reviews*, 23(7–8), 901–918. <https://doi.org/10.1016/j.quascirev.2003.06.021>
- McPhaden, M. J., Zebiak, S. E., & Glantz, M. H. (2006). ENSO as an integrating concept in Earth Science. *Science*, 314(5806), 1740–1745. <https://doi.org/10.1126/science.1132588>
- Moussas, X., Polygiannakis, J. M., Preka-Papadema, P., & Exarhos, G. (2005). Solar cycles: A tutorial. *Advances in Space Research*, 35(5), 725–738. <https://doi.org/10.1016/j.asr.2005.03.148>
- Mudelsee, M. (2002). TAUEST: A computer program for estimating persistence in unevenly spaced weather/climate time series. *Computational Geosciences*, 28(1), 69–72. [https://doi.org/10.1016/s0098-3004\(01\)00041-3](https://doi.org/10.1016/s0098-3004(01)00041-3)
- Mudelsee, M. (2014). *Climate time series analysis: Classical statistical and bootstrap methods* (2nd ed.). Springer.
- Ólafsdóttir, K. B., & Mudelsee, M. (2014). More accurate, calibrated bootstrap confidence intervals for estimating the correlation between two time series. *Mathematical Geosciences*, 46(4), 411–427. <https://doi.org/10.1007/s11004-014-9523-4>
- Osterberg, E. C., Mayewski, P. A., Fisher, D. A., Kreutz, K. J., Maasch, K. A., Sneed, S. B., & Kelsey, E. (2014). Mount Logan ice core record of tropical and solar influences on Aleutian low variability: 500–1998 AD. *Journal of Geophysical Research- Atmospheres*, 119(19), 11–189. <https://doi.org/10.1002/2014jd021847>
- Pierrehumbert, R. T. (2010). *Principles of planetary climate*. Cambridge University Press.
- Rozanski, K., Araguas-Araguas, L., & Gonfiantini, R. (1992). Relation between long-term trends of oxygen-18 isotope composition of precipitation and climate. *Science*, 258(5084), 981–985. <https://doi.org/10.1126/science.258.5084.981>
- Schulz, M., & Mudelsee, M. (2002). REDFIT: Estimating red-noise spectra directly from unevenly spaced paleoclimatic time series. *Computational Geosciences*, 28(3), 421–426. [https://doi.org/10.1016/s0098-3004\(01\)00044-9](https://doi.org/10.1016/s0098-3004(01)00044-9)
- Shen, C. C., Wu, C. C., Cheng, H., Edwards, R. L., Hsieh, Y. T., Gallet, S., et al. (2012). High-precision and high-resolution carbonate ²³⁰Th dating by MC-ICP-MS with SEM protocols. *Geochimica et Cosmochimica Acta*, 99, 71–86. <https://doi.org/10.1016/j.gca.2012.09.018>
- Sigl, M., Winstrup, M., McConnell, J. R., Welten, K. C., Plunkett, G., Ludlow, F., et al. (2015). Timing and climate forcing of volcanic eruptions for the past 2,500 years. *Nature*, 523(7562), 543–549. <https://doi.org/10.1038/nature14565>
- Spötl, C. (2011). Long-term performance of the Gasbench isotope ratio mass spectrometry system for the stable isotope analysis of carbonate microsamples. *Rapid Communications in Mass Spectrometry*, 25(11), 1683–1685. <https://doi.org/10.1002/rcm.5037>
- Stevenson, S., Fox-Kemper, B., Jochum, M., Neale, R., Deser, C., & Meehl, G. (2012). Will there be a significant change to El Niño in the twenty-first century? *Journal of Climate*, 25(6), 2129–2145. <https://doi.org/10.1175/jcli-d-11-00252.1>
- Takahashi, T., Sutherland, S. C., Wanninkhof, R., Sweeney, C., Feely, R. A., Chipman, D. W., et al. (2009). Climatological mean and decadal change in surface ocean pCO₂, and net sea–air CO₂ flux over the global oceans. *Deep Sea Research Part II: Topical Studies in Oceanography*, 56(8–10), 554–577. <https://doi.org/10.1016/j.dsr2.2008.12.009>
- Vecchi, G. A., Clement, A., & Soden, B. J. (2008). Examining the tropical Pacific's response to global warming. *Eos*, 89(9), 81–83. <https://doi.org/10.1029/2008eo090002>
- Wang, B., Luo, X., Yang, Y. M., Sun, W., Cane, M. A., Cai, W., et al. (2019). Historical change of El Niño properties sheds light on future changes of extreme El Niño. *Proceedings of the National Academy of Sciences of the United States of America*, 116(45), 22512–22517. <https://doi.org/10.1073/pnas.1911130116>
- Western Regional Climate Center. Klawock climate summary. Retrieved from wrcc.dri.edu/
- Wilcox, P. S., Dorale, J. A., Baichtal, J. F., Spötl, C., Fowell, S. J., Edwards, R. L., & Kovarik, J. L. (2019). Millennial-scale glacial climate variability in southeastern Alaska follows Dansgaard-Oeschger cyclicity. *Scientific Reports*, 9, 1–8. <https://doi.org/10.1038/s41598-019-44231-1>
- Wilcox, P. S., Mudelsee, M., Spötl, C., & Edwards, R. L. (2022). WA-21-6-A and WB-21-5-A speleothem geochemistry [Dataset]. PANGAEA. <https://doi.org/10.1594/PANGAEA.949778>
- Wiles, G. C., Barclay, D. J., Calkin, P. E., & Lowell, T. V. (2008). Century to millennial-scale temperature variations for the last two thousand years indicated from glacial geologic records of Southern Alaska. *Global and Planetary Change*, 60(1–2), 115–125. <https://doi.org/10.1016/j.gloplacha.2006.07.036>
- Wu, C. J., Krivova, N. A., Solanki, S. K., & Usoskin, I. G. (2018). Solar total and spectral irradiance reconstruction over the last 9000 years. *Astronomy and Astrophysics*, 620, A120. <https://doi.org/10.1051/0004-6361/201832956>
- Yates, F. (1951). The influence of statistical methods for research workers on the development of the science of statistics. *Journal of the American Statistical Association*, 46(253), 19–34. <https://doi.org/10.2307/2280090>

References From the Supporting Information

- Rubino, M., Etheridge, D. M., Thornton, D. P., Howden, R., Allison, C. E., Francey, R. J., et al. (2019). Revised records of atmospheric trace gases CO₂, CH₄, N₂O, and δ¹³C-CO₂ over the last 2000 years from Law Dome, Antarctica. *Earth System Science Data*, 11(2), 473–492. <https://doi.org/10.5194/essd-11-473-2019>